

Stacking-Fault Energy and Anti-Invar Effect in FeMn Alloys

Andrei Reyes-Huamantínco*

*Chair of Atomistic Modeling and Design of Materials, University of Leoben and
Materials Center Leoben Forschung GmbH, A-8700 Leoben, Austria*

Peter Puschnig and Claudia Ambrosch-Draxl

Chair of Atomistic Modeling and Design of Materials, University of Leoben, A-8700 Leoben, Austria

Oleg E. Peil

I. Institute for Theoretical Physics, University of Hamburg, Germany

Andrei V. Ruban

Applied Materials Physics, Royal Institute of Technology, SE-10044 Stockholm, Sweden

(Dated: June 4, 2018)

Based on state-of-the-art density-functional-theory methods we calculate the stacking-fault energy of the paramagnetic random Fe-22.5at.%Mn alloy between 300–800 K. We estimate magnetic thermal excitations by considering longitudinal spin-fluctuations. Our results demonstrate that the interplay between the magnetic excitations and the thermal lattice expansion is the main factor determining the anti-Invar effect, the hcp–fcc transformation temperature, and the stacking-fault energy, which is in excellent agreement with measurements.

The intrinsic stacking-fault (SF) is one of the simplest planar defects of the crystal lattice. It is characterized by a fault in the usual ABC stacking sequence of the fcc structure, $\dots ABCAB|ABC\dots$, which resembles locally the stacking sequence of the hcp structure. The energy to create a stacking-fault, the stacking-fault energy (SFE), is related to the ductility of the material, but the connection between the SFE and the plastic deformation mechanism has so far only been recognized empirically, for instance, in high-Mn steels [1, 2]. Nevertheless, the existence of such a connection provides a unique opportunity for a first-principles theory to be a part of intelligent design of new materials, and in particular high-performance steels, since the SFE is an atomic-scale property readily accessible via *ab initio* methods.

The *ab initio* calculation of the SFE in real alloys at finite temperature presents two main complications: First, the proper description of the atomic-scale structure of multicomponent alloys is complicated because the atomic configuration of alloy components is usually unknown, and, moreover, it is still quite cumbersome to model. Second, the accurate treatment of the thermal excitations of lattice vibrations and magnetic fluctuations in alloys still remains a challenge for any theoretical approach. The magnetic fluctuations are particularly important in fcc and hcp Fe-based alloys, which are weakly itinerant magnets. In particular, this concerns the technologically important Fe-(20-30) at.%Mn alloys, which exhibit both Invar and anti-Invar effects, as well as martensitic transformations and shape memory effects [3, 4].

Special attention is given to the fcc Fe-22.5 at.% Mn, which exhibits the lowest room-temperature SFE of the fcc Fe-Mn alloys [5], and thus is of particular interest for the automotive industry. This alloy undergoes a

structural transformation between γ -austenite (fcc) and ϵ -martensite (hcp) which, on cooling, is characterized by the martensite start temperature, $M_s = 375$ K [6] and, on heating, by the austenite start temperature, $A_s = 450$ K [6]. Important is that the Néel temperatures of both fcc (360 K [3]) and hcp (230 K [7]) are below M_s and A_s , which implies that the fcc–hcp transformation occurs in the paramagnetic state. In addition, the anti-Invar effect, or enhanced thermal lattice expansion, that has been correlated to the magneto-volume coupling [4], also takes place in the paramagnetic state. It is, thus, clear that methods capable of treating the paramagnetic state in a sufficiently reliable fashion are required for a proper description of any finite-temperature properties in this system.

In this Letter, we study the SFE of the Fe-22.5 at.% Mn binary alloy between 300–800 K, using a simple but powerful model based on density-functional theory to take into account spin fluctuations of Fe and Mn atoms, which allows us to obtain excellent agreement with experimental data [5]. The key feature of the methodology used is the capability to describe the strong magneto-volume coupling at finite temperature. We show then that the magneto-volume coupling is responsible for the anti-Invar effect and the temperature dependence of the SFE in the Fe-22.5at.%Mn alloy.

Two recent *ab initio* calculations of the SFE in FeMn alloys [8, 9], that were done at zero-K, failed to reproduce the finite-temperature experimental values even qualitatively. The main motivation of this work is to show that the accurate treatment of the thermal excitations of the magneto-volume coupling is essential for the calculation of the temperature-dependent SFE for the fcc Fe-based alloys, in particular Fe-22.5at.%Mn.

The SFE is evaluated using the axial next-nearest neighbor Ising (ANNNI) model [10]: $SFE(T) = G^{hcp}(T) + 2G^{dhcp}(T) - 3G^{fcc}(T)$, where $G(T)$ is the Helmholtz free energy, and the volume per atom of the *ideal* hcp and dhcp structures is the same as for the fcc structure, implying that only the fcc volume needs to be known. The alloy configuration is assumed to be completely random, which is supported by recent experimental data [11], and the Mn concentration at the SF is the same as in the bulk, i.e., the Suzuki effect [12] is inoperative due to the very slow diffusion of manganese in the austenite phase [13]. The ANNNI model is known to be less accurate than direct supercell calculations, where the SF structure is treated explicitly and the geometry can be relaxed [14]. However, accurate SFE supercell calculations for random alloys in the paramagnetic state are currently impractical.

Generally, the free energy is a difficult quantity to evaluate. Using the coarse graining of the partition function, the contributions from electronic, magnetic, vibrational and configurational excitations can be separated out based on their different time scales. Clearly, the entropy contribution from magnetic excitations in the paramagnetic state can be significant and needs to be assessed. As for the vibrational entropy, there are currently no available theoretical tools to determine it accurately in paramagnetic random alloys. However, its contribution to the free energy *differences* required to evaluate the SFE has been argued to be small [15]. The configurational entropy does not contribute to the SFE in the case of a completely random alloy. Lastly, we regard the effect of the local lattice relaxations to be negligible since the atomic radii of iron and manganese are similar.

Thus, the magnetic excitations seem to be the main entropy contributor to the SFE. The relevant part of the Helmholtz free energy per site is then determined as $G(T) = F_{el}(T) - TS_{mag}(T)$, where $F_{el}(T) \equiv F_{el}[S_{WS}(T), \{\bar{m}_i(T)\}]$ is the electronic part of the free energy, which includes one-electron excitations and depends on the volume given in terms of the Wigner-Seitz (WS) radius $S_{WS}(T)$ and the average local magnetic moments $\bar{m}_i(T)$ of each alloy component i ; the magnetic entropy $S_{mag}(T) \equiv S_{mag}[\{\bar{m}_i(T)\}]$ is determined by the thermal fluctuations of the magnetic moments.

We start with a detailed discussion of the equilibrium volume at finite temperature $S_{WS}(T)$ and its relation to the magnetic moments $\bar{m}_i(T)$. First, we consider the equation of state at $T = 0$ K of the fcc and hcp random alloys in the *paramagnetic* configuration. In order to provide an accurate account of the local environment effects and energetics, we model the alloy by 384-atom supercells consisting of 298 Fe and 86 Mn atoms distributed randomly on the underlying fcc and hcp lattices, i.e., the alloy composition is $\text{Fe}_{0.776}\text{Mn}_{0.224}$. The DFT self-consistent total energy calculations are done in the disordered local moment (DLM) [16] configuration by

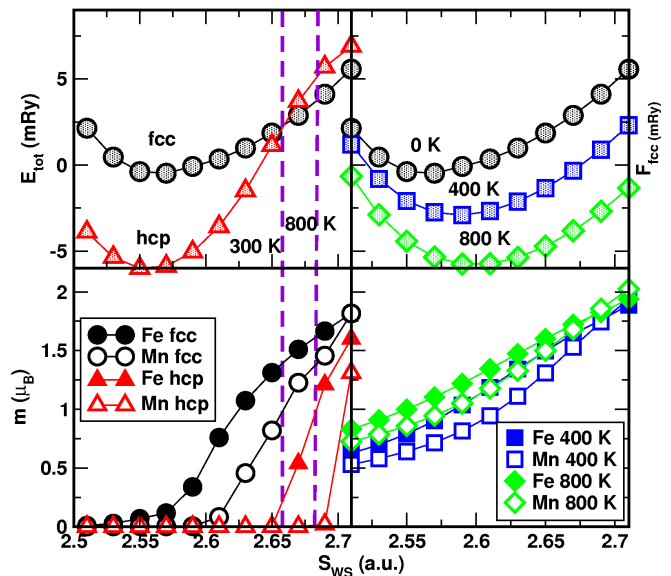


FIG. 1. (Color online) Total energies (upper-left panel) and zero-K DLM magnetic moments (lower-left panel) of Fe and Mn in fcc (circles) and hcp (triangles) $\text{Fe}_{0.776}\text{Mn}_{0.224}$, as function of volume. Two dashed vertical lines show the *experimental* WS radii for this alloy at 300 and 800 K [6, 23]. Helmholtz free energies (upper-right panel) and finite-temperature DLM moments (lower-right panel) of the fcc $\text{Fe}_{0.776}\text{Mn}_{0.224}$ alloy at 400 K (squares) and 800 K (diamonds). The total energy of the $\text{Fe}_{0.776}\text{Mn}_{0.224}$ alloy at zero-K is shown by filled circles.

using the locally self-consistent Green's function (LSGF) method [17, 18] implemented within the exact muffin-tin orbital method combined with the full-charge density technique (EMTO-FCD) [19], called LSGF-EMTO [20].

In the upper-left and lower-left panels of Fig. 1, we show, respectively, the total energies and the DLM local magnetic moments of Fe and Mn as a function of the WS radius for the fcc and hcp $\text{Fe}_{0.776}\text{Mn}_{0.224}$ alloys. We obtain a zero-K fcc equilibrium WS radius, 2.563 a.u., which is much smaller than the room-temperature experimental value, 2.658 a.u. [23], indicated by the dashed vertical line in Fig. 1 [24]. Our zero-K result is in agreement with a recent full-potential supercell calculation, 2.574 a.u. [9], while at variance with a previous EMTO-FCD study, 2.605 a.u. [25]. The latter calculation, however, used the frozen-core approximation, a smaller set of k-points, and had a freedom in the choice of unspecified screening parameters, which can explain the disagreement.

From Fig. 1, we realize that both fcc and hcp phases possess a low-spin equilibrium volume and exhibit a low-spin (LS)–high-spin (HS) transition with increasing WS radii, indicative of the anti-Invar behavior [26]. In addition, the fcc structure becomes more stable than hcp above 2.660 a.u., while simultaneously, a LS hcp–HS fcc transition takes place, demonstrating the coupling between the structural transformation and anti-Invar behavior in the paramagnetic state, which has been dis-

cussed in the literature [26].

At finite temperature, the Helmholtz free energy must be calculated instead of the total energy. The electronic single-particle excitations are described via the Fermi function, while we use the simplest model to describe the longitudinal spin-fluctuations (LSF) in the DLM state. Specifically, we prescribe to each site p in the supercell, having DLM magnetic moment m_p , the entropy $S_{mag} = k_B \ln(m_p + 1)$. The value of m_p is determined by the minimization of the Helmholtz free energy, and in this way, it corresponds to the average magnitude of the magnetic excitations in the DLM state. We note that a more elaborate approach to the treatment of LSF will be used below for the calculation of the SFE.

We have calculated the free energy as a function of the WS radius at 400 and 800 K using LSGF-EMTO, taking into account the LSF as described above. Compared with the zero-K result, the minima of the free energy curves are significantly shifted towards larger volumes upper-right panel in Fig. 1), which is caused by the drastic increase of the magnetic moments due to the LSF (lower-right panel in Fig. 1). From these data, one can estimate $S_{WS}(T)$ by taking into account the vibrational entropy using the Debye-Grüneisen (DG) model [27]. We obtain 2.650 and 2.698 a.u. at 400 and 800 K, respectively, in agreement with the corresponding experimental $S_{WS}(T)$, 2.662 and 2.682 a.u., estimated from X-ray diffraction (XRD) [23] and dilatometric measurements [6].

We also obtain, however, a very large isotropic Grüneisen constant, about 4, and a strongly overestimated value of the thermal-expansion coefficient, which shows that the DG model cannot be used for the quantitative determination of $S_{WS}(T)$ in systems with a large magnetically-induced anharmonicity. Nevertheless, the model shows the strong magneto-volume coupling in this system and allows us to capture qualitatively the crucial feature of the anti-Invar effect, namely, enhanced thermal lattice expansion caused by the so-called moment-volume instabilities [26], i.e., the thermally activated LS low-volume–HS high-volume transition.

The results show that the magneto-volume coupling is an essential feature of the FeMn alloy, and it is, thus, important to have accurate values of $S_{WS}(T)$, and the average local magnetic moment of each alloy component i , $\bar{m}_i(T) \equiv \bar{m}_i[T; S_{WS}(T)]$, at a given temperature T , for a proper description of the system. There are no theoretical methods available to accurately calculate $S_{WS}(T)$ for paramagnetic random alloys, but it can be measured. The situation is, however, the opposite with respect to the magnetic moments $\bar{m}_i(T)$ in the paramagnetic state, which are difficult to measure,

but can be calculated by the procedure described below. We, therefore, combine the values of $S_{WS}(T)$ estimated from the XRD [23] and dilatometric measurements [6] with the theoretically evaluated values of $\bar{m}_i(T)$ to obtain the free energy and finally the SFE at finite

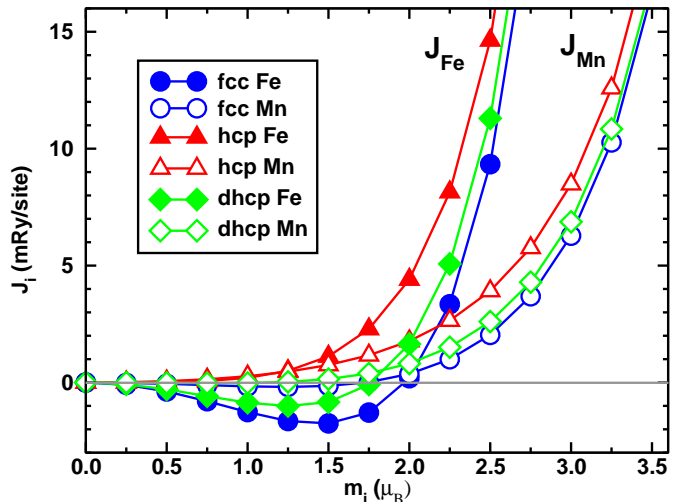


FIG. 2. (Color online) The energy of the LSF, J_i , obtained for different structures, at the fcc $S_{WS}(T = 360 \text{ K}) = 2.660 \text{ a.u.}$ [6, 23], in the EMTO-FCD calculations.

temperatures.

To this end, we proceed to a more elaborate treatment of the LSF and determine $\bar{m}_i(T)$ following the approach in Ref. [28] generalized to the case of a binary alloy. In this procedure, $\bar{m}_i(T)$ are evaluated as the thermodynamic averages of the fluctuating magnetic moments of iron and manganese at a corresponding temperature. For that purpose we assume that the free energy is dominated by single-site magnetic fluctuations in the paramagnetic DLM state. In this case, a Hamiltonian describing the LSF can be defined as $H_{mag} = \sum_i J_i(m_i)c_i$, with $i = \text{Fe, Mn}$, where $J_i(m_i)$ is the energy necessary to excite the magnetic moment m_i of the i th alloy component. In calculating $J_{Fe(Mn)}$, we fix one of the magnetic moments, $m_{Fe(Mn)}$, while letting another, $m_{Mn(Fe)}$, relax.

In Fig. 2 we show the results for $J_i(m_i)$ obtained for fcc $S_{WS}(T = 360 \text{ K}) = 2.660 \text{ a.u.}$ [6, 23] in the EMTO-FCD calculations [29]. In all the cases, J_i have very shallow minima indicating low-energetic accessibility of spin fluctuations, with large variety of the magnetic moments, which reflects the weak itinerant nature of magnetism in this system. The minima of the $J_i(m_i)$ define the equilibrium magnetic moments in the DLM ground state, $m_i^{DLM} \equiv \bar{m}_i(T = 0)$, and we obtain $(m_{Fe}^{DLM}, m_{Mn}^{DLM}) = (1.4, 1.1)\mu_B$ for the fcc, $(0.0, 0.0)\mu_B$ for the hcp, and $(1.2, 0.8)\mu_B$ for the dhcp structures, respectively. Note that these m_i^{DLM} are close to those in the lower-left panel of Fig. 1, at $S_{WS} = 2.660 \text{ a.u.}$, that have been obtained at zero-K in the LSGF-EMTO calculations.

At finite temperature T , the average magnetic moments, $\bar{m}_i(T)$, are readily obtained from the J_i by a simple Monte Carlo integration for each component. In doing so, we assume the complete coupling between lon-

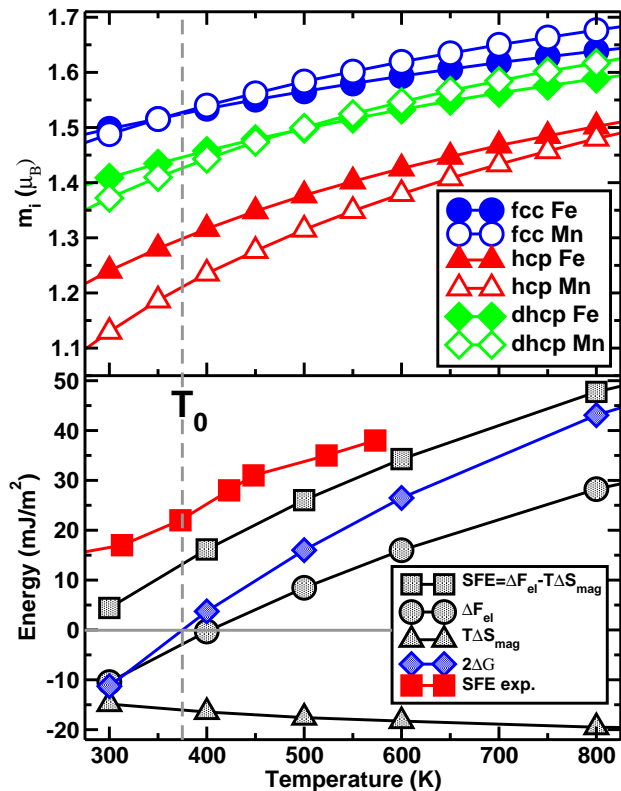


FIG. 3. (Color online) Average magnetic moments of Fe and Mn in different structures (upper panel), and the SFE and its components (lower panel) as a function of temperature. Vertical line indicates the theoretical estimate of the hcp–fcc phase transition.

gitudinal and transverse fluctuations, i.e., the magnitude of the local magnetic moment is determined by its x , y , and z -projections, when integrating over the classical spin phase space. The results are shown in the upper panel of Fig. 3 for different structures in the temperature interval of 300–800 K, and were obtained using the J_i of Fig. 2. Note that our room-temperature $\bar{m}_i(T)$ for the fcc phase is in agreement with neutron diffraction room-temperature measurements of the average moment per site in fcc Fe-30at.%Mn, $1.5 \mu_B$ [31].

Finally, in order to obtain the SFE, we use the calculated $\bar{m}_i(T)$ of Fig. 3 together with the experimental fcc $S_{WS}(T)$ in the free energy calculations of the fcc, hcp and dhcp structures. In the lower panel of Fig. 3 one can readily see that despite a small quantitative discrepancy with the experimental data [5], the temperature dependence of the SFE is nicely reproduced. Moreover, the entropic, $T\Delta S_{mag}(T)$, and electronic free energy, $\Delta F_{el}(T)$, contributions behave quite differently with temperature, with the latter being fully responsible for the temperature dependence of the SFE. The entropic contribution, on the other hand, just shifts (although quite substantially) the

value of the SFE towards the experimental value. This result is contrasted with earlier results by Vitos *et al.* for FeCrNi alloys [15], where the temperature dependence of the SFE was found to be determined solely by the magnetic excitations.

A detailed scrutiny of the sensitivity of the SFE to the values of $S_{WS}(T)$ and $m_i(T)$ enables us to establish the crucial role that thermal excitations and magneto-volume coupling play in the behavior of the SFE. In particular, neglecting the temperature dependence of either the volume, S_{WS} , or the magnetic moments results, respectively, in a largely underestimated value of the SFE, -250 mJ/m^2 at 300 K, when using the equilibrium theoretical zero-K S_{WS} and $m_i(T)$ from Fig. 3, or in an overestimated value of 150 mJ/m^2 at 300 K with the experimental $S_{WS}(T)$ and zero-K m_i^{DLM} .

The obtained free energies allow us also to investigate the structural stability by examining the so-called driving force $\Delta G(T) = G^{hcp}(T) - G^{fcc}(T)$. Our value of the transition temperature, determined by the condition $\Delta G(T_0) = 0$, is 375 K, which is obtained using the ideal c/a ratio and the same atomic volume for the hcp phase as for the fcc one. It is in reasonable agreement with the experimental estimate $T_0^{\text{exp}} \approx (M_s + A_s)/2 = 412 \text{ K}$ [6].

We would like also to remark on the importance of including the dhcp term to the expression for the SFE. In the axial nearest-neighbor Ising (ANNI) model, the SFE is equal to $2\Delta G$. The comparison of the SFE calculated using the next-nearest-neighbor model and $2\Delta G$ in Fig. 3 makes clear that the contribution of the dhcp structure is important for the quantitative description of the SFE.

In summary, our results demonstrate that the interplay between the LSF magnetic excitations and the thermal lattice expansion is the main factor determining the anti-Invar effect, the hcp–fcc transformation temperature, and the SFE in the paramagnetic random Fe-22.5at.%Mn alloy. In principle, this strong sensitivity of the SFE with respect to the quite elusive thermal effects of the magneto-volume coupling makes theoretical studies in magnetic alloys rather difficult. At the same time, we have clearly demonstrated that the accurate account of important thermal contributions within the DFT *ab initio* approach allows not only to obtain a good quantitative agreement with experiment but also to identify mechanisms dominating the formation and stability of the SF at finite temperatures. The formalism presented here can be further generalized to the case of austenitic stainless steels, which are many-component systems with the presence of strong atomic short-range order and local lattice relaxation effects, thereby opening a perspective of the intelligent design of new high-performance materials.

A.R.H., P.P., and C.A.D. acknowledge the financial support by the COMET K2 Centre MPPE, Böhler Special Steels, and Voestalpine AG. A.V.R. is grateful to the Swedish Research Council (VR), Hero-m centrum and the ERC grant for financial support.

* a.huamantinco@mcl.at

- [1] O. Grassel, L. Kruger, G. Frommeyer, and L. W. Meyer, *Int. J. Plasticity* **16**, 1391 (2000).
- [2] G. Frommeyer, U. Brux and P. Neumann, *ISIJ Int.* **43**, 438 (2003).
- [3] V. T. Witusiewicz, F. Sommer and E. J. Mittemeijer, *J. Phase Equilibria Diffusion* **4**, 346 (2004).
- [4] T. Schneider, M. Acet, B. Rellinghaus, E. F. Wassermann, and W. Pepperhoff, *Phys. Rev. B* **51**, 8917 (1995).
- [5] P. Y. Volosevich, V. N. Gridnev, and Y. N. Petrov, *Fiz. Metal. Metalloved.* **42**, 372 (1976).
- [6] S. Cotes, M. Sade, and A. Fernandez Guillermet, *Metalurgical Mat. Trans. A* **26**, 1957 (1995). In Fig. 10, there is an obvious typo in the scale of the vertical axis, which is an order of magnitude too large.
- [7] H. Ohno and M. Mekata, *J. Phys. Soc. Jpn.* **31**, 102 (1971).
- [8] S. Kibey, J. B. Liu, M. J. Curtis, D. D. Johnson, and H. Sehitoglu, *Acta Mater.* **54**, 2991 (2006).
- [9] A. Dick, T. Hickel, and J. Neugebauer, *Steel Res. Int.* **80**, 603 (2009).
- [10] P. J. H. Denteneer and W. van Haeringen, *J. Phys. C Solid State Phys.* **20**, L883 (1987).
- [11] J. Martinez, S. M. Cotes, and J. Desimoni, *Phys. Status Solidi B* **246**, 1366 (2009).
- [12] H. Suzuki, *J. Phys. Soc. Jpn.* **17**, 322 (1962).
- [13] Y. Ueshima, S. Mizoguchi, T. Matsumiya, and H. Kajioka, *Metall. Trans. B* **17**, 845 (1986).
- [14] H. Li, L. Romaner, R. Pippan, and C. Ambrosch-Draxl (in preparation).
- [15] L. Vitos, P. A. Korzhavyi, and B. Johansson, *Phys. Rev. Lett.* **96**, 117210 (2006).
- [16] B. L. Gyorffy, A. J. Pindor, J. Staunton, G. M. Stocks, and H. Winter, *J. Phys. F Met. Phys.* **15**, 1337 (1985).
- [17] I. A. Abrikosov, S. I. Simak, B. Johansson, A. V. Ruban, and H. L. Skriver, *Phys. Rev. B* **56**, 9319 (1997).
- [18] O.E. Peil, A.V. Ruban, and B. Johansson, submitted to PRB.
- [19] L. Vitos, *Computational Quantum Mechanics for Materials Engineers* (Springer-Verlag, London, 2007).
- [20] The local interaction zone in the LSGF-EMTO calculations included the first two coordination shells in the case of the fcc structure and the first three coordination shells in the case of the hcp one. Other details, also relevant for the EMTO-FCD calculations are as follows: The partial waves have been expanded up to $l_{max} = 3$. The integration over the Brillouin zone has been performed using k-mesh grids of 31x31x31 for fcc, 30x30x16 for hcp, and 30x30x8 for dhcp structures. The self-consistent electronic density calculations have been done using the local spin-density approximation (LSDA) [21], while the total energy has been obtained in the generalized gradient approximation (GGA) [22].
- [21] J. P. Perdew and Y. Wang, *Phys. Rev B* **45**, 13244 (1992).
- [22] J. P. Perdew, K. Burke, and M. Ernzerhof, *Phys. Rev. Lett.* **77**, 3865 (1996).
- [23] C.-M. Li, F. Sommer, and E. J. Mittemeijer, *Mat. Sci. Engineering A* **325**, 307 (2002).
- [24] The experimental fcc data is available below M_s because the martensitic transformation is not complete, as found in earlier experiments [31].
- [25] T. Gebhardt, D. Music, B. Hallstedt, M. Ekholm, I. A. Abrikosov, L. Vitos, and J. M. Schneider, *J. Phys. Condens. Mat.* **22**, 295402 (2010).
- [26] V.L. Moruzzi, *Phys. Rev. B* **41**, 6939 (1990).
- [27] V.L. Moruzzi, J.F. Janak, and K. Schwarz, *Phys. Rev. B* **37**, 790 (1988).
- [28] A. V. Ruban, S. Khmelevskiy, P. Mohn, and B. Johansson, *Phys. Rev. B* **75**, 054402 (2007).
- [29] The details of the EMTO-FCD calculations are the same as in the LSGF-EMTO calculations [20], except from the fact that the isomorphous model for the alloy has been used with the on-site screening constant [30] obtained from the corresponding LSGF calculations. At $S_{WS} = 2.660$ a.u. the α screening constants [30] are found to be 0.8143, 0.8120, and 0.8354 for the fcc, hcp, and dhcp structures, respectively.
- [30] A. V. Ruban and H. L. Skriver, *Phys. Rev. B* **66**, 024201 (2002); A. V. Ruban, S. I. Simak, P. A. Korzhavyi, and H. L. Skriver, *Phys. Rev. B* **66**, 024202 (2002).
- [31] H. Umeyashi, and Y. Ishikawa, *J. Phys. Soc. Jpn.* **21**, 1281 (1966).